Research Article | Vol. 2, No. 5 / 15 May 2019 / OSA Continuum 1754

Superresolution optical nanopatterning at low light intensities using a quantum yield-matched photochrome

APRATIM MAJUMDER,[1,3,*] LEVI BOURKE,[1,3] TRISHA L. ANDREW,[2] AND RAJESH MENON[1]

[1] *Department of Electrical and Computer Engineering, University of Utah, Salt Lake City, Utah 84112, USA*
[2] *Department of Chemistry, University of Massachusetts, Amherst, MA 01003, USA*
[3] *These authors contributed equally to this work*
[*] *apratim.majumder@utah.edu*

Abstract: Absorbance-modulation-optical lithography (AMOL) uses the opposing reactions between two isomeric states (absorbing and transparent) of a photochrome to confine light to sub-diffraction limited dimensions. The extent of light confinement is controlled by the ratio of the intensities of the confining and the exposing beams. Traditionally, high intensity in the confining beam is required due to the low quantum yield of the corresponding photo-reaction. Here, we report AMOL using low-light intensities, enabled by a novel photochrome with well-matched quantum yields. We provide rigorous simulations and experiments to demonstrate ~ λ/4.5 feature-sizes at approximately 1/4th the light intensities required in conventional AMOL.

1. Introduction

The widespread adoption of nanotechnology [1,2] has required the development of a multitude of nanopatterning techniques. However, optical-projection photolithography has remained the workhorse of high-volume manufacturing in the semiconductor industry for almost five decades. The resolution achievable in conventional photolithography is limited by the far-field diffraction limit [3]. To overcome this limit, a variety of techniques have been developed including (but not limited to): self-assembly [4], nanoimprint [5], plasmonic [6] and near-field lithography [7]. There have been demonstrations of resolution improvement by Contrast Enhancement Materials (CEM) that use an absorbing material as a top-layer above the photoresist to increase the resolution and reduce the full-width half-maximum (FWHM) of the point spread function (PSF) of the exposing beam spot. [8,9] In comparison to CEMs, the absorbance modulation layer (AML) in Absorbance-Modulation-Optical Lithography (AMOL) behave much the same way. However, in the case of the CEM, for a fixed thickness of a CEM layer, the absorption of the CEM layer cannot be modulated. Since AMOL works by the competing action of the two isomeric forms of the photochromes under the influence of a confining and an exposing beam, the absorption of the layer can be finely tuned using the intensities of the two beams, and hence, the linewidth can in turn be precisely controlled. This has been demonstrated in this paper. Most importantly, without the recovery of the original opaque state (that is possible only in AMOL), it is very challenging to perform multiple exposures, which is necessary to increase the spatial frequencies in the recorded pattern beyond the far-field diffraction limit. Recently, there has also been a demonstration of sub-diffraction limited patterning in conventional i-line photoresists [10] using an approach inspired by the super-resolution microscopic technique named Stimulated Emission Depletion Microscopy (STED) [11]. However, in this case, a modification of the development procedure is required. Also, the demonstrated line pitch is significantly large (~500 nm, compared to the exposing wavelength of ~365 nm) although individual linewidth is small (~ 60 nm) since the authors exploit the non-linear photoresist exposure at the darkest

#362721 https://doi.org/10.1364/OSAC.2.001754
Journal © 2019 Received 21 Mar 2019; revised 20 Apr 2019; accepted 24 Apr 2019; published 6 May 2019

OSA CONTINUUM

region of the nodes in an interference pattern. This inherently limits the period of the exposed lines to be significantly large while also eliminating the possibility of multiple patterning of the photoresist. Neither of these are a concern to the technique described in this work. However, all these approaches suffer from disadvantages ranging from requiring exotic materials to very poor process yields. It is to be noted that AMOL is an alternative super-resolution lithography technique that could overcome these limitations. [12–15].

AMOL is a maskless nanopatterning technique that employs a photochromic absorbance-modulation layer (AML) above a conventional photoresist (PR) film. The AML is comprised of a photochromic material that interconverts between two states based on the wavelength of illumination, with one state being transparent and the other opaque to the exposing wavelength ($\lambda_1 = 325$ nm) as shown schematically in Fig. 1(a). The AML is simultaneously illuminated with a confining beam at $\lambda_2 = 647$ nm patterned as a standing wave and a uniform exposing beam at $\lambda_1 = 325$ nm as indicated in Fig. 1(b) [12,13]. The λ_2 photons convert the AML to an isomeric form, which absorbs λ_1, while the λ_1 photons convert the AML to another isomeric form, which is transparent to λ_1. If the powers of the two beams are balanced appropriately, an absorption pattern is created in the AML, as well as a sub-diffraction limited aperture at the interface of the AML and the PR. λ_1 photons can penetrate through this aperture and the resulting pattern can then be recorded in the underlying PR. The two opposing reactions determine the widths of the transparent regions in the AML (and subsequently the widths of the patterns created in the PR). By increasing the intensity of the confining beam relative to that of the exposing beam, it is possible to reduce these widths to be far smaller than those dictated by the far-field diffraction limit. It is to be noted that since the exposing beam (λ_1) is uniform and not patterned, whereas only the confining beam (λ_2) carries a spatial pattern, the successful recording of gratings in the PR demonstrate the proof of principle of AMOL. The AML is simply a polymer top layer that is doped with the photochromic molecules. It does not require any special treatment and does not affect or complicate the photoresist processing and the overall lithographic process in any significant manner. Addition of top layers with minimal processing has also been fairly commonly adopted in the lithographic industry. At the same time, the photochromes are fully CMOS compatible and can be easily deposited using chemical vapor deposition (CVD) techniques like evaporation, which is more suitable in CMOS industry, in addition to wet processing like spin-coating, as is demonstrated here.

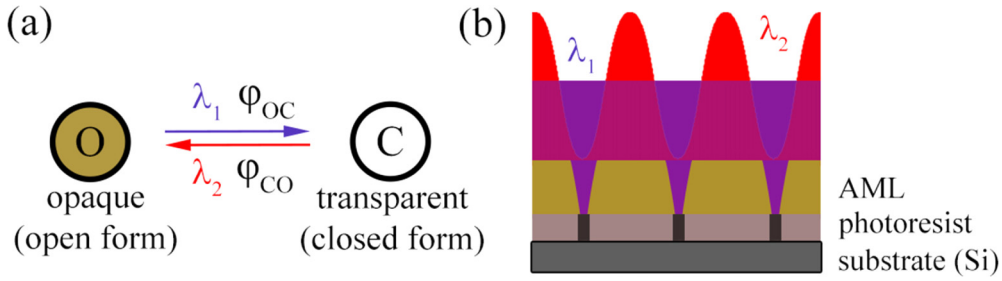

Fig. 1. Schematic of AMOL showing (a) the photoreactions and (b) simultaneous illumination of the AML by uniform λ_1 and standing waves λ_2 leading to the creation of a dynamic absorption pattern in a layer above the conventional photoresist film. λ_1 photons penetrate through the sub-diffraction limited aperture at the interface of the AML and PR to expose the PR.

However, since the quantum yield of the "confining" reaction is several orders of magnitude lower than that of the "exposing" reaction, the intensity of the confining beam needs to be correspondingly higher than that of the exposing beam. This is problematic for fast patterning and also to achieve very small feature sizes. Here, we show that the structure of the photochrome

OSA CONTINUUM

can be tailored [16] such that the photochemical quantum yields of the two opposing reactions are better matched and that a structure-optimized photochrome allows for super-resolution lithography to be performed at much lower intensities of both beams. There are a number of available photochromes that could have been chosen for our application. The choice of BTE and cPTE was due to their absorption peaks being (1) one at the photoresist exposure wavelength (325 nm) and (2) the other at a readily available laser source in our laboratory (647 nm).

2. Description of photochromes

Two different diarylethene photochromes were employed in this work, (a) 1,2-bis(5,5' –dimethyl-2,2'-bithiophen-4-yl) perfluorocyclopent-1-ene (referred to as BTE), whose usage in AMOL has been reported previously [12–15] and the newly optimized photochrome, (b) 1,2-bis(2-methyl-5-(p-cyanophenyl)-3-thienyl)-3,3,4,4,5,5-hexafluoro-1-cyclopentene (referred to as cPTE) [16]. Figure 2(a) shows the molecular structures of the open and closed isomeric forms of cPTE. cPTE was synthesized following a previously-reported procedure [17] and the open form thus accessed was confirmed to display the same ^{1}H and ^{13}C nuclear magnetic resonance spectra, and high-resolution mass spectra as previously reported.

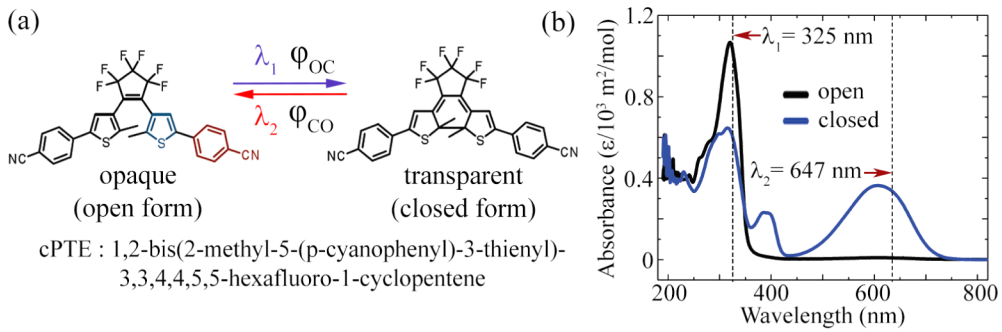

Fig. 2. (a) Molecular structure of photochrome cPTE and (b) Absorption spectra of cPTE. In our experiments, $\lambda_1 = 325$ nm and $\lambda_2 = 647$ nm.

The absorption spectra for the closed and open forms of cPTE are shown in Fig. 2(b). The wavelengths for the exposing and confining beams were chosen to correspond approximately with the absorption peaks of the open forms ($\lambda_1 = 325$ nm) and the closed forms ($\lambda_2 = 647$ nm), respectively. In its open form, the electron-rich bithiophene arms of BTE can freely rotate to minimize steric repulsion and are twisted out of the plane of the central, electron-poor perfluorocyclopentene ring, precluding advantageous hyper-conjugative interactions between these two moieties. In contrast, the rigidly planar closed form of BTE allows for hyperconjugation, which particularly stabilizes this isomer and increases the activation barrier for ring opening to the comparatively destabilized open form. These unique characteristics lead to a large mismatch in the quantum yields for the photochemical conversion of one isomer to the other: BTE has a quantum yield of the closed-to-open (φ_{CO}) reaction of 8.8×10^{-4}, which is several orders of magnitude lower than that for the open-to-closed (φ_{OC}) reaction, 0.24. In cPTE, the cyanophenyl moiety found in both arms of the photochrome is both more sterically bulky and electron deficient, as compared to a thiophene moiety. The steric bulk of the cyanophenyl moiety hinders free rotation of these arms (as compared a bithiophene arm) and, when mixed inside a polymer matrix, the two arms of cPTE are kinetically trapped in one rotomeric state. This process reduces the overall quantum yield of the photochemical ring closing reaction in cPTE as compared to BTE. The electron deficient nature of the cyanophenyl moiety of each arm in cPTE draws electron density away from each thiophene ring and globally prevents hyperconjugation with the

OSA CONTINUUM

perfluorocyclopentene ring in either the open or closed isomer, meaning that the quantum yield of the reverse ring opening reaction is not attenuated. These two effects, in synergy, mean that the quantum yields of the ring opening and closing reactions are closer in value than those of BTE. As mentioned earlier, the quantum-yield mismatch was a drawback in the case of BTE and necessitated the use of very high intensity ratios between the two beams when using BTE for AMOL. Previously, we demonstrated light confinement to about $\lambda_1/10$ with intensity ratio of almost 8000 [12,13,18].

3. Simulation results

We previously described a numerical tool that was developed to rigorously model AMOL using finite-element methods [14,16]. Here, we utilized this tool to first analyze the impact of the optimized photochrome on the resolution achievable in AMOL. Also, we previously showed that the polarizations of the confining and exposing beams must be transverse electric (TE) and transverse magnetic (TM), respectively [19]. We utilized the model described in Ref. [14], in conjunction with the following parameters. The photoresist is modelled as a variable thickness material with a complex refractive index value of 1.6–0.5i at λ_1. The parameter values for BTE have been reported before [12–14]. We followed the same procedure as outlined in Ref. [12] to obtain the parameter values for cPTE. The parameter values for BTE are as follows: $\varepsilon_{1O} = 3113.6\ m^2/mol$, $\varepsilon_{1C} = 1052.1\ m^2/mol$, $\varepsilon_{2O} = 15.8\ m^2/mol$, $\varepsilon_{2C} = 2003.5\ m^2/mol$, $\varphi_{OC} = 0.24$, $\varphi_{CO} = 8.8 \times 10^{-4}$. The corresponding values for the cPTE are: $\varepsilon_{1O} = 3240\ m^2/mol$, $\varepsilon_{1C} = 1920\ m^2/mol$, $\varepsilon_{2O} = 0$, $\varepsilon_{2C} = 960\ m^2/mol$, $\varphi_{OC} = 6.5 \times 10^{-2}$, $\varphi_{CO} = 1.4 \times 10^{-3}$. The thickness of the photochromic layer is 100 nm and initial concentration of photochromes in the AML = 6000 mol/m^3.

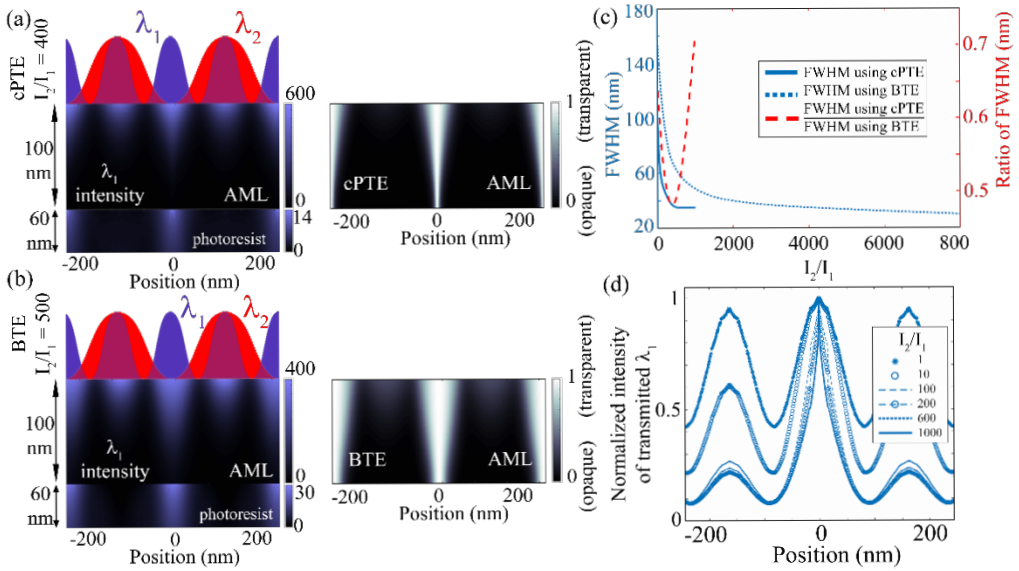

Fig. 3. Simulation results: Light intensity distribution for the exposing UV beam (λ_1) for an AML composed of (a) cPTE and of (b) BTE. λ_1 confinement is much superior in cPTE for even a lower intensity ratio ($I_1/I_2 = 400$) when compared to BTE ($I_1/I_2 = 500$). (c) FWHM scaling trend for cPTE compared to BTE. (d) AMOL PSF for cPTE with increasing intensity ratio.

OSA CONTINUUM

To prove the effectiveness of using a better quantum yield-matched photochrome, simulations using both BTE and cPTE were conducted with the same conditions (Fig. 3). Figs. 3(a) and 3(b) show the 2D full field simulation of the exposing beam (λ_1 = 325 nm) within the AML and PR layers. The cPTE (Fig. 3(a)) example has tighter confinement in the AML (and subsequently in the PR) compared to the BTE (Fig. 3(b)) for an even lower intensity ratio ($I_2/I_1 = 400$ in the case of cPTE, compared to 500 in the case of BTE). The distribution of the photochromic species is shown to the right of the EM fields distribution for both cases, again demonstrating the superior light confinement of cPTE at low intensity ratios. Finally, in Fig. 3(c) we plot the feature width in the PR defined as full-width at half-maximum (FWHM) of the intensity distribution of λ_1 within the PR, with respect to the light intensity ratios as a metric for comparison of the performance of the two photochromic species. The FWHM reduces as a function of the ratio, I_2/I_1 significantly faster when using cPTE than when using BTE. In other words, one requires a significantly smaller intensity ratio to achieve a given feature width with cPTE than with BTE. In Fig. 3(d), we plot the corresponding intensity distributions at λ_1 inside the PR, where the light confinement at increasing intensity ratios is evident. As expected, this confinement occurs at lower intensity ratios when compared to the case of using BTE. It is interesting to note that similar scale enhancement factors are desirable in sphere assisted lithography using lasers [21].

4. Experimental results

A Mach-Zehnder interferometer (MZI) with the confining beam ($\lambda_2 = 647$ nm) was used to create the standing-wave pattern. A schematic of the experimental setup is shown in Fig. 4(e). The period of the λ_2 standing wave = $\lambda_2/2n\sin\theta$, where n is the refractive index of the medium that the light is travelling through and θ is the half-angle of interference as shown in Fig. 4(e). Here, n = 1, and $\theta = 45$ °. The period of λ_2 standing wave is calculated to be 457 nm. It has been demonstrated previously through extensive simulations [14] as well as experiments [15] that the effect of changing the period of the exposing beam on the final AMOL point spread function (PSF) in the photoresist is negligible.

A UV LED ($\lambda_1 = 325$ nm) was used as the exposing beam. The samples were comprised of a Si wafer coated with a monolayer of HMDS, on top of which the layer of photoresist was spin-coated. The chemical synthesis yields cPTE in crystalline powder form. Hence, in order for the cPTE to be spin cast on to the sample to create the AML, it was required to be suspended in a polymer matrix. Previously [9,16], we have used Polystyrene as this polymer for the BTE molecule. However, since cPTE is not well soluble in polystyrene, we resorted to use Poly(methyl methacrylate) (PMMA). Conversely, cPTE may also be deposited as a top layer using a CVD process like evaporation, that is standard in the CMOS industry. In our case, we chose spin-coating and wet-processing due to its relative simplicity and high speed of processing samples. cPTE was dissolved in PMMA at 96% by weight in a 3% by weight of PMMA-in-Anisole solution and spin-coated at 750 rpm, producing a 340 nm thick layer. PMMA has negligible absorbance at the two wavelengths λ_1 and λ_2. The absorbance peaks of PMMA occur below 300 nm [22]. The cPTE layer was separated from the photoresist layer by a thin (~8 nm) barrier layer of polyvinyl alcohol (PVA). The use of a barrier layer increases the linewidth due to diffraction, but is necessary to protect the PR from the cPTE. A 640 nm layer of diluted (1:3) Shipley S1813 PR was produced by spinning at 2000rpm. The intensity of the λ_2 beam was fixed at approximately 220 W/m^2, while the intensity of the λ_1 beam was varied between 0.8-0.11 W/m^2, in order to achieve different intensity ratios. After the AMOL exposures, the AML was stripped away by dissolving in Anisole, by immersing the sample in a beaker of Anisole for 15-20 s. Next, the barrier layer was removed by simply rinsing the sample in DI-water for 30 s. Finally, the photoresist was developed by immersing in a suitable developer (TMAH based or NaOH based) for 1 min. The sample was lastly, rinsed in DI water for 15 s and air-dried. Finally,

OSA CONTINUUM

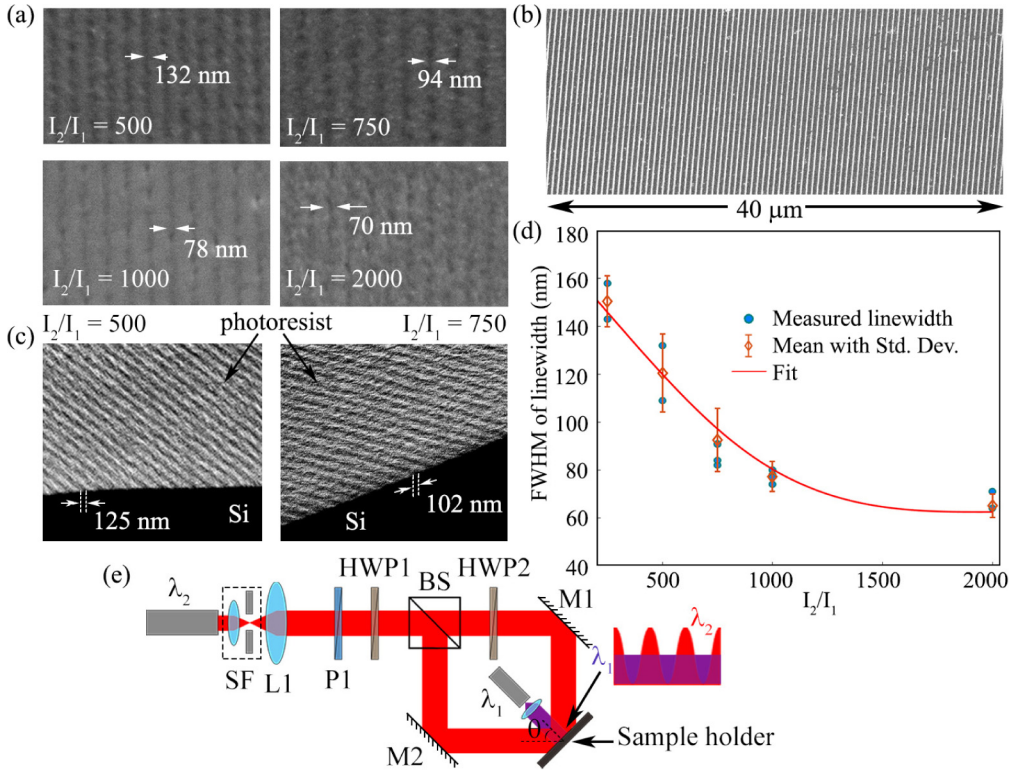

Fig. 4. cPTE AMOL Experimental results. Scanning electron micrographs showing (a) PR patterning at different intensity ratios (b) Large area patterning and (c) Titled cross-sections of PR (d) Feature-scaling trend showing variation of FWHM of linewidth vs intensity ratio. (e) Schematic of the experimental setup showing a modified Mach-Zehnder interferometer setup used to perform AMOL experiments. λ_2 source is a Kr-ion laser at wavelength 647 nm, SF = spatial filter, L1 = collimating lens, P1 = linear polarizer, HWP1 and HWP2 = half wave plates used for making the power in the two arms of the λ_2 beam equal, BS = beam splitter, M1 and M2 = guiding mirrors, λ_1 source is UV LED at wavelength 325 nm.

the samples were coated with 2-3 nm of Au/Pd in a desktop sputter coater system (PECS) for imaging in a scanning electron microscope (FEI Quanta).

The scanning-electron micrographs shown in Figs. 4(a-c) show periodic lines in the developed PR. Their linewidths decreased with increasing intensity ratio as shown in Fig. 4(d). FWHM of approximately 70 nm can be produced with an intensity ratio of ~2000 with cPTE, while this was achieved only at a ratio of about 8000 with BTE [20]. It must be noted that uniform illumination was used for the exposing beam and the only spatial pattern was in the confining beam. Hence, with respect to the confining beam wavelength, the feature size ~ $\lambda_2/9$ and with respect to the exposing beam ~ $\lambda_1/4.5$. One may use a PR that can be exposed by λ_2 to take advantage of this scheme by using λ_1 as the confining beam and λ_2 as the exposing beam. We have demonstrated this before [15] with BTE. A schematic of the modified Mach-Zehnder interferometer used for the lithographic experiments is shown in Fig. 4(e). These results confirm the efficacy of using a photochrome with matched quantum yields in AMOL. It is to be noted that although the experiments demonstrated here use a modified interferometric setup to generate alternating peaks and troughs in the confined beam, the technique of AMOL is not limited to using only interferometers to generate patterns. In the past, we have shown that it is possible

OSA CONTINUUM

to achieve arbitrary (aperiodic) patterns using dichromats and techniques involving zone plate array (ZPAL) systems to achieve focal spots and nodes in the exposing beam [23,24]. These systems may be readily combined with the current materials to achieve aperiodic lithographic patterning, which will be demonstrated in the future. It is to also be noted that the combination of AMOL with 2-photon absorption would lead to an increase in the contrast of the patterning beam. This approach has been pursued with promising results elsewhere [25–28]. However, this will necessitate higher laser intensities, which might lead to slower patterning and related challenges.

5. Conclusions

Here, we demonstrated using simulations and experiments, that resolution beyond the far-field diffraction limit may be achieved in optical lithography via absorbance modulation at low light intensities by matching the quantum yields of the two opposing photochemical reactions involved. Low light intensities are critical to increase the lithographic throughput as well as to simplify the experimental system. Further co-optimization of the photochromic layer, the photoresist and process conditions should yield even higher resolutions with better pattern contrasts enabling fast nanopatterning of complex geometries. One of the important advantages of our approach is the relative compatibility with existing photoresists and lithographic processes, which should enable its rapid adoption.

Funding

National Science Foundation (NSF) (1054899, 1309041, 1400142, 1609146).

Acknowledgments

We would like to thank Brian Baker, Brian van Devener and Paulo Perez at the University of Utah for assistance with sample preparation and imaging.

References

1. K. Jain, C. G. Wilson, and B. J. Lin, "Ultrafast high-resolution contact lithography using excimer lasers," Proc. SPIE **334**, 259–262 (1982).
2. M. Rothschild, "A Roadmap for Optical Lithography," Opt. Photonics News **21**(6), 26–31 (2010).
3. E. Abbé, "Beitragezurtheorie des mikroskops und der mikroskopischenwahrnehmung," Arch. Mikrosk. Anat. Entwichlungsmech **9**(1), 413–418 (1873).
4. J. Wu, Y. Liu, Y. Guo, S. Feng, B. Zou, H. Mao, C.-H. Yu, D. Tian, W. Huang, and F. Huo, "Centimeter-Scale Subwavelength Photolithography Using Metal-Coated Elastomeric Photomasks with Modulated Light Intensity at the Oblique Sidewalls," Langmuir **31**(17), 5005–5013 (2015).
5. S. V. Sreenivasan, "Nanoimprint Lithography Steppers for Volume Fabrication of leading-edge Semiconductor Integrated Circuits," Microsyst. Nanoeng. **3**, 17075 (2017).
6. W. Srituravanich, N. Fang, C. Sun, Q. Luo, and X. Zhang, "Plasmonics Lithography," Nano Lett. **4**(6), 1085–1088 (2004).
7. R. J. Blaikie, D. O. S. Melville, and M. M. Alkaisi, "Super-resolution near-field lithography using planar silver lenses: A review of recent developments," Microelectron. Eng. **83**(4-9), 723–729 (2006).
8. S. Geary, J. Thompson, and E. S. Capsuto, "Contrast enhancement materials for yield improvement in submicron i-line lithography," *Proc. SPIE 4689, Metrology, Inspection, and Process Control for Microlithography XVI*, 1017–1026 (2002).
9. C. A. Mack, "Photoresist Process Optimization," KTI Microelectronics Seminar, Interface **87**, 153–167 (1987).
10. D. B. Miller, A. M. Jones, and R. R. McLeod, "Super-resolution critical dimension limits of positive tone i-line photoresists," *Proc. SPIE 10544, Advanced Fabrication Technologies for Micro/Nano Optics and Photonics XI, 105440N, 105440N-1-10* (2018).
11. G. Vicidomini, P. Bianchini, and A. Diaspro, "STED super-resolved microscopy," Nat. Methods **15**(3), 173–182 (2018).
12. T. L. Andrew, H.-Y. Tsai, and R. Menon, "Confining light to deep subwavelength dimensions to enable optical Nanopatterning," Science **324**(5929), 917–921 (2009).
13. A. Majumder, F. Masid, B. J. Pollock, T. L. Andrew, and R. Menon, "Barrier Free Absorbance Modulation for Superresolution Optical Lithography," Opt. Express **23**(9), 12244–12250 (2015).

OSA CONTINUUM

14. A. Majumder, P. J. Helms, T. L. Andrew, and R. Menon, "A Comprehensive Simulation Model of the performance of Photochromic films in Absorbance-Modulation-Optical-Lithography," AIP Adv. **6**(3), 035210 (2016).
15. A. Majumder, X. Wan, F. Masid, B. J. Pollock, T. L. Andrew, and R. Menon, "Reverse Absorbance-Modulation-Optical-Lithography for Optical patterning at low light levels," AIP Adv. **6**(6), 065312 (2016).
16. A. Majumder, X. Wan, B. J. Pollock, T. L. Andrew, and R. Menon, "Modelling the Performance of Photochromic Thin Films to Achieve Super-resolution Nanopatterning by Absorbance Modulation at Low Light Intensity," in *Imaging and Applied Optics 2016*, (Optical Society of America, 2016), paper IM4F.4.
17. J. J. D. de Jong, L. N. Lucas, R. Hania, A. Pugzlys, R. M. Kellogg, B. N. Feringa, K. Duppen, and J. H. van Esch, "Photochromic properties of Perhydro- and Perfluorodithienylcyclopentene Molecular Switches," Eur. J. Org. Chem. **2003**(10), 1887–1893 (2003).
18. F. Masid, T. L. Andrew, and R. Menon, "Optical Patterning of Features with spacing below the Far-field Diffraction limit using Absorbance Modulation," Opt. Express **21**(4), 5209–5214 (2013).
19. J. E. Foulkes and R. J. Blaikie, "Influence of polarization on absorbance modulated subwavelength grating structures," J. Vac. Sci. Technol. B **27**(6), 2941–2946 (2009).
20. A. Majumder, "Super-Resolution Optical Nanopatterning Beyond the Far-Field Diffraction Limit Using Photochromic Molecules and Absorbance Modulation Optical Lithography," Doctoral Dissertation, University of Utah (2018).
21. L. N. D. Kallepalli, D. Grojo, L. Charmasson, P. Delaporte, O. Utéza, A. Merlen, A. Sangar, and P. Torchio, "Long range nanostructuring of silicon surfaces by photonic nanojets from microsphere Langmuir films," J. Phys. D: Appl. Phys. **46**(14), 145102 (2013).
22. R. M. Ahmed, "Optical Study on Poly(methyl methacrylate)/Poly(vinyl acetate) Blends," Int. J. Photoenergy **2009**, 1–7 (2009).
23. H.-Y. Tsai, H. I. Smith, and R. Menon, "Reduction of focal-spot size using dichromats in absorbance modulation," Opt. Lett. **33**(24), 2916 (2008).
24. H.-Y. Tsai, S. W. Thomas III, and R. Menon, "Parallel scanning optical nanoscopy with optically confined probes," Opt. Express **18**(15), 16014 (2010).
25. J. Fischer and M. Wegener, "Three-dimensional direct laser writing inspired by stimulated-emission-depletion microscopy," Opt. Mater. Express **1**(4), 614–624 (2011).
26. J. Fischer, J. B. Mueller, J. Kaschke, T. J. A. Wolf, A.-N. Unterreiner, and M. Wegener, "Three-dimensional multi-photon direct laser writing with variable repetition rate," Opt. Express **21**(22), 26244–26260 (2013).
27. R. Wollhofen, J. Katzmann, C. Hrelescu, J. Jacak, and T. A. Klar, "120 nm resolution and 55 nm structure size in STED-lithography," Opt. Express **21**(9), 10831–10840 (2013).
28. Z. Gan, Y. Cao, R. A. Evans, and M. Gu, "Three-dimensional deep sub-diffraction optical beam lithography with 9 nm feature size," Nat. Commun. **4**(1), 2061 (2013).